arXiv:1601.06822v1 [physics.flu-dyn] 22 Jan 2016

Solitary wave shoaling and breaking in a regularized Boussinesq system

Amutha Senthilkumar
Department of Mathematics, University of Bergen
Postbox 7803, 5020 Bergen, Norway
Email: amutha.senthilkumar@math.uib.no
Telephone number: (47) 55584858

January 27, 2016

Abstract

A coupled BBM system of equations is studied in the situation of water waves propagating over decreasing fluid depth. A conservation equation for mass and a wave breaking criterion valid in the Boussinesq approximation is found. A Fourier collocation method coupled with a 4-stage Runge-Kutta time integration scheme is employed to approximate solutions of the BBM system. The mass conservation equation is used to quantify the role of reflection in the shoaling of solitary waves on a sloping bottom. Shoaling results based on an adiabatic approximation are analyzed. Wave shoaling and the criterion of breaking solitary waves on a sloping bottom is studied. To validate the numerical model the simulation results are compared with those obtained by Grilli et al. [16] and a good agreement between them is observed. Shoaling of solitary waves of two different types of mild slope model systems in [8] and [30] are compared, and it is found that each of these models works well in their respective regimes of applicability.

Key words: Coupled BBM system, Shoaling rates, Mass conservation law

1 Introduction

Model equations for free surface water waves propagating in a horizontal channel of uniform depth have been widely studied for many years. Boussinesq models incorporate the lowest-order effects of nonlinearity and frequency dispersion as corrections to the linear long wave equation. These models are widely used for describing the propagation of non-linear shallow water waves near coastal regions. In Boussinesq theory, it is important to assume that water is incompressible, inviscid and the flow is irrotational. There are two important parameters which are the nonlinearity, the ratio of amplitude to depth, represented by $\alpha = a/h_0$, and the dispersion, the ratio of depth to wavelength, represented by $\beta = h_0^2/l^2$. As explained in detail in [5], the Boussinesq approximation is valid only when both α and β are small and have the same order of magnitude.

The more realistic situation of uneven bottom profile is fundamental to studies of ocean wave dynamics in coastal regions. Several authors [14, 18, 20, 29, 39, 42] have included the effect of smooth and slowly varying bottom topographies in both Boussinesq and shallow water theory. The 'classical' Boussinesq model was applied to shallow water of uneven bottom in two horizontal dimensions by Peregrine [35], who used depth-averaged velocity as a dependent variable and

derived the system

$$\eta_t + \nabla \cdot [(h+\eta)\bar{\mathbf{u}}] = 0, \tag{1a}$$

$$\bar{\mathbf{u}}_t + \nabla\eta + (\bar{\mathbf{u}} \cdot \nabla)\bar{\mathbf{u}} - \frac{h}{2}\nabla(\nabla \cdot (h\bar{\mathbf{u}}_t)) + \frac{h^2}{6}\nabla(\nabla \cdot (\bar{\mathbf{u}}_t)) = 0, \tag{1b}$$

where the independent variable $\mathbf{x} = (x, y)$ represents the position, $\eta = \eta(\mathbf{x}, t)$ represents the deviation of the free surface from its rest position at time t, $\mathbf{u} = \mathbf{u}(\mathbf{x}, z, t)$ denotes the horizontal velocity of the fluid at some height, while $\bar{\mathbf{u}}$ denotes the depth-averaged velocity

$$\bar{\mathbf{u}} = \frac{1}{h+\eta}\int_{-h}^{\eta} \mathbf{u}\, dz, \tag{2}$$

and the bottom is $z = -h(\mathbf{x})$.

Several improved Boussinesq-type models have been developed, starting with Madsen et al. [26], Nwogu [31] and Wei et al. [41], among others. Madsen et al. [26] achieved an improved linearized model by rearranging higher-order terms in the classical momentum equations, which are formally equivalent to zero within the accuracy of the model. Nwogu [31] demonstrated the flexibility obtained by using the velocity at an arbitrary distance from the still water level as the velocity variable. Wei et al. [41] used Nwogu's approach to derive a fully nonlinear extensions of Boussinesq equations which further extended the range of validity of Boussinesq models without the weak nonlinearity restriction. It is worth mentioning that in [8, 30] the Boussinesq model (1) has been extended to moving bottom topography, where the bottom topography depends on x, y and t. In the paper [30], a BBM-type system (see [3]) has been derived and solved numerically using a finite element method. One way in which the BBM system differs from Peregrine's Boussinesq system is in the way it is amenable to numerical integration. Indeed, it is much easier to define a stable numerical approximation to a system of BBM type than to other Boussinesq systems, such as the Peregrine system. On the other hand, the Peregrine system features exact mass conservation while mass conservation in the BBM-type systems is only approximate. Nevertheless, in the current work, we use a system of BBM type for numerical convenience.

The main contribution of the present paper is an in-depth study of wave reflection in a shoaling analysis based on of Boussinesq systems such as (1). Wave shoaling is the effect by which surface waves propagating shorewards experience a decrease in the water depth. The study of shoaling waves is of importance in the nearshore areas, and in the design of coastal structures. As part of our analysis, we formulate an approximate mass balance law associated to the Boussinesq scaling, such as developed for flat bottoms in [1]. We also extend the wave breaking criterion from [4] to the case of uneven beds. The mass balance equation is used in quantifying wave reflection due to the bottom slope, and the wave breaking criterion is used to determine an approximate termination point for the shoaling curves. A significant amount of literature has focused on the use of nonlinear shallow water equations to analyse long wave shoaling on a mildly sloping beach, and both experimental and numerical investigations have been carried out. However, reflection has not been quantified.

Many experimental studies, including the early studies [6, 17] were aimed partly at comparison with classical shoaling laws such as the laws of Green and Boussinesq. However, most experimental work on wave shoaling has shown that actual shoaling curves vary considerably from the predictions of both Green's and Boussinesq's law. Grilli et al.[16] solved the full Euler equations by direct numerical integration and this work compares their shoaling results with the numerical solution obtained from the present work.

Wave breaking is also important in studying nearshore area phenomena and is also important for the study of tsunami propagation in coastal regions, because solitary waves are often used to model steep surface waves shoaling on beaches. An enormous literature also exists about breaking waves in a number of situations, including shoaling, wave breaking in open bodies of water, and

breaking induced by a wavemaker (see [12, 37], for instance). Chou and Ouyang [9, 10] and Chou et al. [11] discussed the criterion for the breaking of solitary waves on different slopes using the boundary element method to simulate the process of wave breaking. Using the fully nonlinear potential flow wave model, Grilli et al. [16] derived a criterion for wave breaking. In this paper, a different criterion of breaking solitary waves on a sloping bottom of BBM-type system is derived based on previous work in [4]. Characteristics such as the breaking index, the waveheight, the water depth and the maximum particle velocity at the breaking point are studied and the breaking indices are compared with those obtained by Grilli et al. [16] and Chou et al. [11].

The present paper is organized as follows. In Section 2, the outline for the derivation of the coupled BBM-type system [30] is given, and also the mass balance equations and the wave breaking criterion are derived. In Section 3, the coupled BBM-type system is solved numerically using a Fourier collocation method coupled with a 4-stage Runge-Kutta time integration scheme. We validate the convergence of the numerical scheme and demonstrate the effectiveness of the numerical method applied to our model system in simulations of solitary wave shoaling on a sloping bottom. Mass reflection, shoaling and wave breaking are studied numerically. This paper compares two models; the coupled BBM-type system derived by Chen [8] and the one in Mitsotakis [30] with respect to evolution of solitary waves. This comparison is concerned with initial wave profiles and wave shoaling on slopes that correspond to unidirectional propagation. Finally, a short conclusion is given in Section 4.

2 Derivation of the system

The main model system to be used here belongs to a family of models derived in Mitsotakis [30]. Let us briefly outlined the derivation. In order to obtain the Boussinesq system, the full water wave problem is used. A Cartesian coordinate system (x, z) is considered, with the x- axis along the still water level and z- axis pointing vertically upwards. The fluid domain is bounded by the sea bed at $z = -h(x)$ and the free surface $z = \eta(x, t)$. Then the system of Euler equations for potential flow theory in the presence of a free surface is used. The derivation of the Boussinesq system is only briefly sketched. For a full derivation, the interested reader may consult [8] and [30]. The variables are non-dimensionalized using following scaling:

$$\tilde{x} = \frac{x}{l}, \quad \tilde{z} = \frac{z}{h_0}, \quad \tilde{t} = \frac{\sqrt{gh_0}t}{l}, \tag{3a}$$

$$\text{and} \quad \tilde{h} = \frac{h}{h_0}, \quad \tilde{\eta} = \frac{\eta}{a}, \quad \tilde{\phi} = \frac{h_0}{al\sqrt{gh_0}}\phi, \tag{3b}$$

where tilde ($\tilde{}$) denotes non-dimensional variables, and h_0, l and a denote characteristic water depth, wavelength and wave amplitude, respectively.

Consider a standard asymptotic expansion of the velocity potential ϕ and using the Laplace condition ($\triangle\phi = 0,\ -h < z < \eta$), write the velocity potential $\tilde{\phi}$ in the simplest form

$$\tilde{\phi} = \tilde{\phi}^{(0)} + \frac{\tilde{z}}{1!}\tilde{\phi}^{(1)} + (-\beta)\left[\frac{\tilde{z}^2}{2!}\frac{\partial^2}{\partial\tilde{x}^2}\tilde{\phi}^{(0)} + \frac{\tilde{z}^3}{3!}\frac{\partial^2}{\partial\tilde{x}^2}\tilde{\phi}^{(1)}\right] + (\beta^2)\left[\frac{\tilde{z}^4}{4!}\frac{\partial^4}{\partial\tilde{x}^4}\tilde{\phi}^{(0)} + \frac{\tilde{z}^5}{5!}\frac{\partial^4}{\partial\tilde{x}^4}\tilde{\phi}^{(1)}\right] + \mathcal{O}(\beta^3), \tag{4}$$

which is a series solution with only two unknown functions $\tilde{\phi}^{(0)}$ and $\tilde{\phi}^{(1)}$. Then the velocity field can be expressed as

$$\tilde{u}(\tilde{x}, \tilde{z}, \tilde{t}) = \tilde{\phi}_{\tilde{x}} = \hat{u} + \beta\left[\frac{\tilde{z}}{1!}\hat{w}_{\tilde{x}} - \frac{\tilde{z}^2}{2!}\hat{u}_{\tilde{x}\tilde{x}}\right] + \beta^2\left[-\frac{\tilde{z}^3}{3!}\hat{w}_{\tilde{x}\tilde{x}\tilde{x}} + \frac{\tilde{z}^4}{4!}\hat{u}_{\tilde{x}\tilde{x}\tilde{x}\tilde{x}}\right] + \mathcal{O}(\beta^3), \tag{5a}$$

$$\tilde{w}(\tilde{x}, \tilde{z}, \tilde{t}) = \tilde{\phi}_{\tilde{z}} = \beta\left[\hat{w} - \tilde{z}\hat{u}_{\tilde{x}}\right] + \beta^2\left[-\frac{\tilde{z}^2}{2!}\hat{w}_{\tilde{x}\tilde{x}} + \frac{\tilde{z}^3}{3!}\hat{u}_{\tilde{x}\tilde{x}\tilde{x}}\right] + \mathcal{O}(\beta^3), \tag{5b}$$

where $\hat{u}$ and $\hat{w}$ are the velocities at $\tilde{z}=0$ and given by $\hat{u}=\tilde{\phi}_{\tilde{x}}^{(0)},\ \hat{w}=(1/\beta)\tilde{\phi}^{(1)}$.

In order to establish the relation between $\hat{u}$ and $\hat{w}$, use the bottom kinematic boundary condition ($\phi_z+h_x\phi_x=0$ at $z=-h$), which has the following form after substituting the above asymptotic expressions:

$$\hat{w}=-(\tilde{h}\hat{u})_{\tilde{x}}+\beta\frac{\partial}{\partial\tilde{x}}\left(\frac{\tilde{h}^3}{3!}\hat{u}_{\tilde{x}\tilde{x}}-\frac{\tilde{h}^2}{2!}(\tilde{h}\hat{u})_{\tilde{x}\tilde{x}}\right)+\mathcal{O}(\beta^2). \tag{6}$$

Now inserting (4), (5) and (6) into free surface boundary conditions, one may derive the following Boussinesq system with variable bottom

$$\hat{u}_{\tilde{t}}+\tilde{\eta}_{\tilde{x}}+\alpha\hat{u}\hat{u}_{\tilde{x}} = \mathcal{O}(\alpha\beta,\beta^2), \tag{7a}$$

$$\tilde{\eta}_{\tilde{t}}+\left(\alpha\tilde{\eta}\hat{u}+\tilde{h}\hat{u}\right)_{\tilde{x}}-\beta\frac{\partial}{\partial\tilde{x}}\left(\frac{\tilde{h}^3}{3!}\hat{u}_{\tilde{x}\tilde{x}}-\frac{\tilde{h}^2}{2!}(\tilde{h}\hat{u})_{\tilde{x}\tilde{x}}\right) = \mathcal{O}(\alpha\beta,\beta^2). \tag{7b}$$

It is emphasized that from the above system, and in terms of $\hat{u}$, one can extend the system in terms of other velocity variables, such as the velocity at an arbitrary z location. In this work we use a trick due to [31]. Namely, a new velocity variable $\tilde{u}^\theta$ defined at an arbitrary water level $\tilde{z}=-\tilde{h}+\theta(\alpha\tilde{\eta}+\tilde{h})$, with $0\le\theta\le1$. Applying the standard techniques of inversion it is not difficult to derive the following expression as an asymptotic formula for $\hat{u}$ in terms of $\tilde{u}^\theta$:

$$\hat{u}=\tilde{u}^\theta+\beta\left(\tilde{h}(\theta-1)(\tilde{h}\tilde{u}^\theta)_{\tilde{x}\tilde{x}}+(\tilde{h})^2(\theta-1)^2\frac{1}{2!}(\tilde{u}^\theta)_{\tilde{x}\tilde{x}}\right)+\mathcal{O}(\alpha\beta,\beta^2). \tag{8}$$

Switching to the variable $\tilde{u}^\theta$, the following expressions are obtained:

$$\tilde{\eta}_{\tilde{t}}=-\left(\tilde{h}\tilde{u}^\theta\right)_{\tilde{x}}+\mathcal{O}(\alpha,\beta),\qquad \tilde{u}^\theta_{\tilde{t}}=-\tilde{\eta}_{\tilde{x}}+\mathcal{O}(\alpha,\beta). \tag{9}$$

Following the methodology in [5], for arbitrary $\mu,\nu\in\mathbb{R}$ and using (9), the following equations are derived

$$(\tilde{h}\tilde{u}^\theta)_{\tilde{x}\tilde{x}}=\mu(\tilde{h}\tilde{u}^\theta)_{\tilde{x}\tilde{x}}-(1-\mu)\tilde{\eta}_{\tilde{t}\tilde{x}}+\mathcal{O}(\alpha,\beta) \tag{10a}$$

$$\tilde{u}^\theta_{\tilde{t}\tilde{x}\tilde{x}}=(1-\nu)\tilde{u}^\theta_{\tilde{t}\tilde{x}\tilde{x}}-\nu\tilde{\eta}_{\tilde{x}\tilde{x}\tilde{x}}+\mathcal{O}(\alpha,\beta) \tag{10b}$$

Using equations (7)-(10) and appropriate expansions, the following system is derived:

$$\tilde{u}^\theta_{\tilde{t}}+\tilde{\eta}_{\tilde{x}}+\alpha\tilde{u}^\theta\tilde{u}^\theta_{\tilde{x}}+\beta\left\{B\tilde{h}\left[(\tilde{h}_{\tilde{x}}\tilde{\eta}_{\tilde{x}})_{\tilde{x}}+\tilde{h}_{\tilde{x}}\tilde{\eta}_{\tilde{x}\tilde{x}}\right]+c\tilde{h}^2\tilde{\eta}_{\tilde{x}\tilde{x}\tilde{x}}-d\tilde{h}^2\tilde{u}^\theta_{\tilde{x}\tilde{x}\tilde{t}}\right\}=\mathcal{O}(\alpha\beta,\beta^2) \tag{11a}$$

$$\tilde{\eta}_{\tilde{t}}+\left(\alpha\tilde{\eta}\tilde{u}^\theta+\tilde{h}\tilde{u}^\theta\right)_{\tilde{x}}+\beta\frac{\partial}{\partial\tilde{x}}\left\{A\tilde{h}^2\left[(\tilde{h}_{\tilde{x}}\tilde{u}^\theta)_{\tilde{x}}+\tilde{h}_{\tilde{x}}\tilde{u}^\theta_{\tilde{x}}\right]+a\tilde{h}^2(\tilde{h}\tilde{u}^\theta)_{\tilde{x}\tilde{x}}-b\tilde{h}^2\tilde{\eta}_{\tilde{x}\tilde{t}}\right\}=\mathcal{O}(\alpha\beta,\beta^2). \tag{11b}$$

The parameters a, b, c and d are the same as in [5], where

$$\begin{aligned} A&=\frac{1}{2}\left[\frac{1}{3}-(\theta-1)^2\right], & B&=1-\theta,\\ a&=\frac{1}{2}\left(\theta^2-\frac{1}{3}\right)\mu, & b&=\frac{1}{2}\left(\theta^2-\frac{1}{3}\right)(1-\mu),\\ c&=\frac{1}{2}\left(1-\theta^2\right)\nu, & d&=\frac{1}{2}\left(1-\theta^2\right)(1-\nu). \end{aligned} \tag{12}$$

Note that the coupled BBM-type system appears in (11) if $\mu=0$ and $\nu=0$. Disregarding terms of order $\mathcal{O}(\alpha\beta,\beta^2)$ and dropping the superscript θ, the system takes the following form in dimensional variables

$$u_t+g\eta_x+uu_x+2Bghh_x\eta_{xx}+Bghh_{xx}\eta_x-dh^2u_{xxt}=0, \tag{13a}$$

$$\eta_t+(\eta u+hu)_x+\frac{\partial}{\partial x}\left\{2Ah^2h_xu_x+Ah^2h_{xx}u-bh^2\eta_{xt}\right\}=0. \tag{13b}$$

Assuming the depth h is constant, the above system reduces to the original coupled BBM system in [5].

2.1 Mass balance

As mentioned in the introduction, the use of the BBM system necessitates the derivation of an approximate mass balance law. The following mass balance derivation is based on the work in [1]. They have already presented mass balance theory for the Boussinesq models with even bottom profile. Since we are interested in varying bottom topography, we provide the following derivation. The integral form of the equation of mass conservation is

$$\frac{d}{dt}\int_{x_1}^{x_2}\int_{-h(x)}^{\eta}\rho\,dz\,dx=\left[\int_{-h(x)}^{\eta}\rho\phi_x\,dz\right]_{x_2}^{x_1}, \tag{14}$$

since there is no mass flux through the bottom or through the free surface. In non-dimensional variables the above relation becomes

$$\frac{d}{d\tilde{t}}\int_{\tilde{x}_1}^{\tilde{x}_2}\int_{-\tilde{h}}^{\alpha\tilde{\eta}}d\tilde{z}\,d\tilde{x}=\left[\int_{-\tilde{h}}^{\alpha\tilde{\eta}}\alpha\tilde{\phi}_{\tilde{x}}\,d\tilde{z}\right]_{\tilde{x}_2}^{\tilde{x}_1}. \tag{15}$$

After integration with respect to $\tilde{z}$ and use of asymptotic expansion of $\tilde{\phi}$, we obtain

$$\int_{\tilde{x}_1}^{\tilde{x}_2}(\alpha\tilde{\eta}+\tilde{h})_{\tilde{t}}\,d\tilde{x}=\alpha\left[\hat{u}(\tilde{h}+\alpha\tilde{\eta})+\frac{\tilde{h}^2}{2!}\beta(\hat{u}\tilde{h})_{\tilde{x}\tilde{x}}-\frac{\tilde{h}^3}{3!}\beta(\hat{u})_{\tilde{x}\tilde{x}}\right]_{\tilde{x}_2}^{\tilde{x}_1}+\mathcal{O}(\alpha\beta,\beta^2). \tag{16}$$

Note that if we take the limit $\tilde{x}_2\to\tilde{x}_1$, where $\tilde{x}_2=x_2/l$ and $\tilde{x}_1=x_1/l$, then we obtain the balance equation (7b). i.e,

$$\frac{\partial}{\partial\tilde{t}}\tilde{M}+\frac{\partial}{\partial\tilde{x}}\tilde{q}_M=\mathcal{O}(\alpha\beta,\beta^2), \tag{17}$$

where

$$\tilde{M}=\alpha\tilde{\eta}+\tilde{h},\quad \tilde{q}_M=\alpha\left[\left(\alpha\tilde{\eta}\tilde{u}^\theta+\tilde{h}\tilde{u}^\theta\right)+\beta(\theta-\tfrac{1}{2})\tilde{h}^2(\tilde{h}\tilde{u}^\theta)_{\tilde{x}\tilde{x}}+\beta\tilde{h}^3(\tfrac{1}{2}(\theta-1)^2-\tfrac{1}{6})(\tilde{u}^\theta)_{\tilde{x}\tilde{x}}\right].$$

The derivation could also be based on the differential form of the mass conservation, such as in [2]. If we use the scalings $M=\rho h_0\tilde{M}$ and $q_M=\rho h_o\sqrt{(gh_0)}\tilde{q}_M$, then the dimensional form of these quantities are

$$M=\rho(\eta+h(x)),\quad q_M=\rho\left[u(h+\eta)+h^2(\theta-\tfrac{1}{2})(hu)_{xx}+\tfrac{1}{2}h^3((\theta-1)^2-\tfrac{1}{3})u_{xx}\right]. \tag{18}$$

Eq. (17) represents the approximate mass balance equation. The net mass transfer to or from a control volume during a time interval $\triangle t$ is equal to the net change (increase or decrease) in the total mass in the control volume during $\triangle t$. In [1], they proved that the maximum error in the conservation of mass is smaller than $\mathcal{O}(\alpha\beta,\beta^2)$ in the case of even bottom profile using a coupled BBM system. In Subsection (3.2) the amount of mass reflection will be computed for different cases.

2.2 Wave breaking in BBM model system

As waves approach the shoreline the wavelength and phase velocity decrease and the wave amplitude grows larger. The wave then crashes onto shore because it becomes too steep for the bottom of the wave to carry it. The breaking of waves mostly depends on wave steepness and beach slope. As explained in [4], if the horizontal velocity near the crest of a wave exceeds the celerity of the

wave, then the wave breaks. Let us denote propagation speed by U and horizontal velocity by u. The horizontal velocity u can be obtained from (5a) and (8):

$$\tilde{u} = \tilde{u}^\theta + \beta\left((\tilde{h}(\theta-1)-\tilde{z})(\tilde{h}\tilde{u}^\theta)_{\tilde{x}\tilde{x}} + ((\tilde{h})^2(\theta-1)^2-\tilde{z}^2)\frac{1}{2!}(\tilde{u}^\theta)_{\tilde{x}\tilde{x}}\right) + \mathcal{O}(\alpha\beta,\beta^2). \tag{19}$$

It is evident that once $u^\theta(x,t)$ is known, (19) can be used to approximate the horizontal velocity at any depth. After neglecting the second-order term, the dimensional form of the equation is given by

$$u = u^\theta + (h(\theta-1)-z)(hu^\theta)_{xx} + (h^2(\theta-1)^2-z^2)\frac{1}{2!}(u^\theta)_{\tilde{x}\tilde{x}}. \tag{20}$$

Wave breaking occurs if

$$u^\theta + (h(\theta-1)-\eta)(hu^\theta)_{xx} + (h^2(\theta-1)^2-\eta^2)\frac{1}{2!}(u^\theta)_{xx} > U. \tag{21}$$

Since the fluid domain depends on the surface profile, the value $z=\eta$ is used to approximate velocities near the surface. It is clear that the solutions $\eta(x,t)$ and $u^\theta(x,t)$ of the system (13) and propagation speed U are needed to find the breaking criterion.

3 Numerical methods

The system (13) has been solved numerically using a Fourier collocation method coupled with a 4-stage Runge-Kutta time integration scheme. For numerical computations, periodic boundary conditions on the domain $[0,L]$ are used. For this the problem is translated to the interval $[0,2\pi]$ using the scaling $u(\lambda x,t)=v(x,t)$, $\eta(\lambda x,t)=\xi(x,t)$ and $h(\lambda x)=h_1(x)$, where $\lambda=\frac{L}{2\pi}$. Then the BBM- system (13) becomes

$$\begin{aligned}
\lambda^3 v_t + \lambda^2 g\xi_x + \lambda^2 vv_x + 2Bgh_1h_{1x}\xi_{xx} + Bgh_1h_{1xx}\xi_x - \lambda d{h_1}^2 v_{xxt} &= 0, \quad x\in[0,2\pi],\\
\lambda^3\xi_t + \lambda^2(\xi v + h_1 v)_x + \frac{\partial}{\partial x}\left\{2A{h_1}^2h_{1x}v_x + A{h_1}^2h_{1xx}v - \lambda b{h_1}^2\xi_{xt}\right\} &= 0, \quad x\in[0,2\pi],\\
v(x,0)=u(\lambda x,0), \quad \xi(x,0)=\eta(\lambda x,0),&\\
v(0,t)=v(2\pi,t), \quad \xi(0,t)=\xi(2\pi,t), \text{ for } t\geq 0.&
\end{aligned}$$

Consider the set of N evenly spaced grid points $x_j=\frac{2\pi j}{N}$, $j=1,...N$ in the interval $[0,2\pi]$ referred to as collocation nodes. The spectral-collocation method is implemented in the physical space by seeking approximate solutions through a global periodic interpolation polynomial of the form

$$v_N(x)=\sum_{j=1}^{N} v_N(x_j)g_j(x), \quad \xi_N(x)=\sum_{j=1}^{N}\xi_N(x_j)g_j(x),$$

where $g_j(x)=\frac{1}{N}\sin\left(\frac{N(x-x_j)}{2}\right)\cot\left(\frac{1}{2}(x-x_j)\right)$ and $v_N(x)$, $\xi_N(x)$ is an interpolation of the function $v(x)$, $\xi(x)$ respectively, i.e., $v_N(x_j)=v(x_j), \xi_N(x_j)=\xi(x_j)$ (see [40], [13]). Moreover, the corresponding Fourier collocation differentiation matrices D_x and D_{xx} are given by

$$D^{(1)}_{ij}=\frac{dg_j}{dx}(x_i)=\begin{cases}\frac{1}{2}(-1)^j\cot(\frac{x_i-x_j}{2}) & i\neq j\\ 0 & i=j\end{cases} \tag{23a}$$

$$D^{(2)}_{ij}=\frac{d^2g_j}{dx^2}(x_i)=\begin{cases}-\frac{(-1)^j}{2\sin^2((x_i-x_j)/2)} & i\neq j\\ \frac{-\pi^2}{3h^2}-\frac{1}{6} & i=j\end{cases} \tag{23b}$$

Then at the collocation points $x = xj$, the system becomes

$$\begin{aligned}\left[\lambda^3 I_N - \lambda b\ D_N diag(h_1^2) D_N\right] \xi_{Nt} &= -\lambda^2 D_N(diag(h_1)v_N) - \lambda^2 D_N(\xi_N v_N) \\ &\quad -D_N(2Ah_1^2 h_{1x} D_N(v_N) + Ah_{1xx}h_1^2 v_N), \\ \left[\lambda^3 I_N - \lambda d\ diag(h_1^2) D_N^{(2)}\right] v_{Nt} &= -\lambda^2 g D_N(\xi_N) - \lambda^2 (0.5) D_N(v_N^2) \\ &\quad -2Bgh_1 h_{1x} D_N^{(2)}(\xi_N) - Bgh_1 h_{1xx} D_N(\xi_N),\end{aligned}$$

where I_N is the unit $N \times N$ matrix and D_N, $D_N^{(2)}$ are square matrices of dimensions $N \times N$ following from (23a) and (23b), respectively and $diag(h_1)$, $diag(h_1^2)$ are the diagonal matrices of h_1 and h_1^2, respectively. This is a system of N ordinary differential equations for ξ_N and also v_N. The system is solved by using a fourth order explicit Runge-Kutta scheme with time step $\triangle t$.

3.1 Convergence study

It is important to verify the convergence of the numerical scheme. This is done following [36]. A numerical method is convergent if the numerically computed solution approaches the exact solution as the step size approaches 0. To test the convergence of these numerical methods, the following discrete L^2 - norm is used

$$\|\xi\|_{N,2}^2 = \frac{1}{N}\sum_{j=1}^{N} |\xi(x_j)|^2,$$

and the corresponding relative L^2 - error is then defined to be

$$\frac{\|\xi - \xi_N\|_{N,2}}{\|\xi\|_{N,2}},$$

where $\xi_N(x_j)$ is the approximated numerical solution and $\xi(x_j)$ is the exact solution at a time T, for $j = 1, 2, \ldots, N$.

Supposing the case of an even bottom, the coupled BBM system features solitary-wave solutions in a closed form if $\theta^2 = \frac{7}{9}$ (see [7]). Since the analysis of the solitary wave shoaling and breaking given here depend on the exact formula for the solitary wave, $\theta^2 = \frac{7}{9}$ is used in the present work. Then the exact solitary wave solutions of system of equations (13) takes the form

$$\eta(x,t) = H_0\ \mathrm{sech}^2(\kappa_0(x - C_0 t)), \tag{25}$$

$$u(x,t) = W_0\ \mathrm{sech}^2(\kappa_0(x - C_0 t)), \tag{26}$$

where h_0 is the undisturbed depth, H_0 is wave amplitude, and the constants W_0, C_0 and κ_0 are given by

$$W_0 = \sqrt{\frac{3g}{H_0 + 3h_0}} H_0, \quad C_0 = \frac{3h_0 + 2H_0}{\sqrt{3h_0(H_0 + 3h_0)}}\sqrt{gh_0} \quad \text{and } \kappa_0 = \frac{3}{2h_0}\sqrt{\frac{H_0}{2H_0 + 3h_0}}.$$

To check the convergence of these methods, we determine the L^2 - error each time for n steps and set the step size as $\triangle t = (t_{max} - t_{min})/n$ for different n values $n = 20, 40, 80, \ldots$ (Table 1) and different number of grid points $N = 256, 512, 1024, \ldots$ (Table 2) in the case of an even bottom topography. A representative result for a wave of amplitude 0.5 is given in Tables 1 and 2. The numerical scheme was implemented in MATLAB. In this calculation, the solution was approximated from $T = 0$ to $T = 5$ and the size of the domain was L=100. In the computations shown in Table 1, $N = 1024$ Fourier modes were used. Table 1 shows fourth-order convergence of

the Runge–Kutta method in terms of the time step $\triangle t$. The 4th-order convergence of the scheme is apparent up to $\triangle t = 0.0039$, when the error became dominated by the spatial discretization and the artificial periodicity. Table 2 shows the results of some computations aimed at validating the spatial convergence of the code. As expected, spectral convergence in terms of the number of spatial grid points N is achieved in these computations. Computations were also performed for other solitary waves with heights between 0.1 and 0.6, and similar results were obtained for these cases.

n	$\triangle t$	L^2 - error	Convergence rate
20	0.2500	5.33e-02	-
40	0.1250	3.93e-03	13.58
80	0.0625	2.39e-04	16.44
160	0.0312	1.44e-05	16.49
320	0.0156	8.89e-07	16.29
640	0.0078	5.50e-08	16.15
1280	0.0039	3.60e-09	15.35
2560	0.0020	1.07e-09	03.36

Table 1: L^2 - error and convergence rate for Runge–Kutta method for different fixed step sizes in case of even bottom profile

N	$\triangle t$	L^2 - error	Convergence rate
256	0.0001	2.3 e-04	-
512	0.0001	2.77e-09	84364.95
1024	0.0001	3.09e-012	896.81
2048	0.0001	5.371e-011	0.05

Table 2: L^2 - error and convergence rate due to spatial discretization in case of even bottom profile

To Indicate the significance of the improvement, Tables 3 and 4 show the results of computing approximate solutions of the inhomogeneous BBM-type system

$$u_t + g\eta_x + uu_x + 2Bghh_x\eta_{xx} + Bghh_{xx}\eta_x - dh^2u_{xxt} = f(x,t), \tag{27a}$$

$$\eta_t + (\eta u + hu)_x + \frac{\partial}{\partial x}\left\{2Ah^2h_xu_x + Ah^2h_{xx}u - bh^2\eta_{xt}\right\} = g(x,t), \tag{27b}$$

where the functions $\eta(x,t) = 0.3\cos(x-t)$ and $u(x,t) = 0.3\sin(x-t)$ are used as the exact solutions and the bottom $h(x) = 0.5 - (0.1)\cos(x)$ is assumed. Then the relative L^2- error for various pairs of combinations between the time step $\Delta t = 0.1/2n$, for $n = 1, 2, 3, ...$; and $N = m \times 64$ for $m = 1, 2, 3, ...$ is calculated. The results are shown in Table 3 and Table 4, where the solutions were approximated from $T = 0$ to $T = 5$. These tables show that the numerical implementation of BBM-type system with periodic bottom function $h(x)$ is correct. Similar results can be obtained for other $2\pi-$periodic functions u, η and $h(x)$.

n	$\triangle t$	L^2 -error	Convergence rate
50	0.1000	1.3046e-05	-
100	0.0500	8.2126e-07	15.89
200	0.0250	5.1277e-08	16.02
400	0.0125	3.2023e-09	16.01
800	0.0063	2.0007e-10	16.01
1600	0.0031	1.2500e-11	16.01
3200	0.0016	9.3000e-13	13.41
6400	0.0008	6.2000e-13	01.51

Table 3: Inhomogeneous BBM-type system (27); L^2 - error and convergence rate due to temporal discretization

N	$\triangle t$	L^2 -error	Convergence rate
64	0.001	9.6-01	-
128	0.001	5.4e-06	176234.99
256	0.001	2.1e-13	26437130.31
512	0.001	6.6e-13	0.31
1024	0.001	6.5e-13	1.007

Table 4: Inhomogeneous BBM-type system (27); L^2 - error and convergence rate due to spatial discretization

3.2 Mass conservation results on a sloping bottom

The effect of depth variations on solitary waves of shallow water wave theory is examined. The BBM system (13) is simulated. In all the numerical results of this subsection we use $N = 1024$, $\theta^2 = \frac{7}{9}$. Mass conservation is used to quantify the role of reflection in the shoaling of solitary waves. Note that the piecewise smooth linear bottom topography is used. To avoid the generation of small spurious oscillations due to the discontinuity in the derivative of the bottom function, it is smoothed near the singular points.

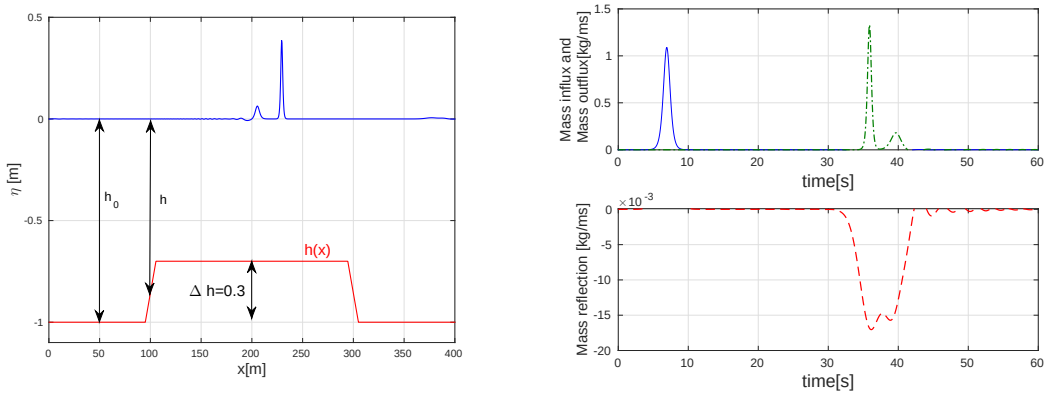

Figure 1: The left panel shows a solitary wave solution for the system (13) with initial amplitude 0.3m at time t=60s. The right panel shows plots of time series of the mass influx at $x = 50m$ (blue solid curve), the mass reflection at $x = 50m$ (red dashed curve) and mass outflux at $x = 150m$ (green dash-dotted curve), per unit span. The results are shown in the numerical domain.

Consider a control volume delimited by the interval $[50, 150]$ on the x-axis. The mass per

unit width contained in this interval is defined by $\int_{50}^{150} M(x,t)\,dx$ and the mass flux through the boundaries of the control volume is defined by $q_M(50,t)$ and $q_M(150,t)$, where M and q_M are given in (18). The quantities M and q_M during the passage of solitary wave are computed. It is observed that the mass outflux is approximately equal to the addition of mass influx and the reflection of the mass. In the right panel of Figure 1, the blue solid curve shows the mass influx at $x = 50m$, the red solid curve shows the mass reflection at $x = 50m$ and the green dotted curve is mass outflux at $x = 150m$. As seen in Figure 1, the mass reflection has negative values.

In Table 5, the results for various amplitudes of the solitary wave are displayed for $\Delta h = 0.3$ on a slope $1 : 35$. Here Δh is the height of the topography. For $\Delta h = 0.3$, the mass influx through the initial boundary of control volume is defined by "Mass influx = $\int_0^{15} q_m(50,t)\,dt$", the mass outflux through the final boundary of control volume is defined by "Mass outflux = $\int_{15}^{60} q_m(150,t)\,dt$" and the mass reflection through the initial boundary of control volume is defined by "Mass reflection = $\int_{15}^{60} q_m(50,t)\,dt$". Note that the time limit may vary for other Δh's. The error is defined by " error = mass outflux - mass reflection - mass influx". It is clear from Table 5, that error tends to 0 as $\alpha = a/h_0$ approaches 0.

In Table 6, the results for various Δh of water level are displayed with an initial amplitude $a = 0.3$ on a slope $1 : 35$. It is clear from Table 5 and Table 6, that the mass conservation holds approximately for the coupled BBM system and the ratio between mass reflection and mass influx is called "mass ratio", which is smaller for smaller Δh.

Amplitude	Mass influx	Mass outflux	Mass reflection	Error
0.2	1.0995	1.0117	-0.0879	0.0001
0.3	1.3856	1.2799	-0.1059	0.0002
0.4	1.6438	1.5236	-0.1204	0.0002
0.5	1.8856	1.7529	-0.1329	0.0002
0.6	2.1166	1.9732	-0.1438	0.0003

Table 5: Error in mass conservation for different waveheights on a slope 1:35 and $\Delta h = 0.3$. The "error = mass outflux - mass reflection - mass influx" quantifies the error in the mass balance law. This table suggest that mass conservation holds approximately.

Δh	Mass influx	Mass outflux	Mass reflection	Mass ratio
0.1	1.3856	1.3535	-0.0320	0.0232
0.2	1.3856	1.3186	-0.0669	0.0483
0.3	1.3856	1.2799	-0.1059	0.0764
0.4	1.3856	1.2358	-0.1500	0.1083
0.6	1.3856	1.1855	-0.2003	0.1446

Table 6: The ratio between mass reflection and mass influx of a solitary wave with initial amplitude $a = 0.3$ on a slope 1:35 for different Δh. Ratio of mass reflection and mass influx is decreasing with decreasing Δh.

The reflection of a small amplitude wave when a solitary wave goes through a slope is defined as "reflection". To find the ratio between reflection and initial solitary wave, the following L^2-norm

$$\|\eta\|^2_{L^2(\mathbb{R})} = \int_{\mathbb{R}} |\eta(x)|^2\,dx,$$

is used.

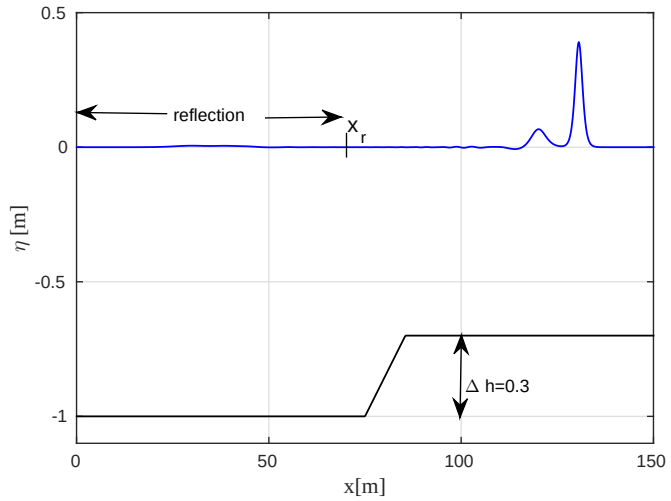

Figure 2: Reflection of solitary waves of initial amplitude $0.2m$ transformation on the slope $S = 1:35$ and $\Delta h = 0.2$ in the physical domain.

To calculate the L^2-norm of initial solitary waves, the value of η is integrated with respect to x on the fluid domain $[0, L]$ at initial time $t = 0$. To determine the L^2-norm of reflected wave, we run the solitary wave on the slope for long enough time to separate the reflection of small wave from solitary wave. The end point of the reflected waves on the $x-$axis is denoted by x_r (see Figure 2). Then the reflected wave is integrated on the interval $[0, x_r]$. And the corresponding "reflection coefficient" is then defined to be

$$\frac{\|\eta \text{ reflection}\|_{L^2([0,x_r])}}{\|\eta \text{ initial at } t=0\|_{L^2([0,L])}}.$$

It is clear from Table 7 that the "reflection coefficient" approaches zero as the slope become more and more gentle.

slope	$\Delta h = 0.3,\ H_0 = 0.3$		$\Delta h = 0.2,\ H_0 = 0.2$		$\Delta h = 0.1,\ H_0 = 0.1$	
	$\|\eta \text{ reflection}\|_{L^2}$	Reflect. coeff.	$\|\eta \text{ reflection}\|_{L^2}$	Reflect. coeff.	$\|\eta \text{ reflection}\|_{L^2}$	Reflect. coeff.
1:35	4.70e-04	1.70e-03	1.76e-04	1.20e-03	2.61e-05	5.19e-04
1:100	1.77e-04	6.40e-04	7.11e-05	4.85e-04	1.45e-05	2.88e-04
1:400	2.82e-05	1.02e-04	1.42e-05	9.69e-05	4.24e-06	8.43e-05
1:800	8.73e-05	3.15e-05	3.04e-06	2.08e-05	3.56e-07	7.08e-06

Table 7: Calculation of the amount of "reflected" waves for different slopes and amplitudes. It shows that the "reflection coefficient" approaches zero, as the slope becomes more and more gentle.

3.3 Evolution of solitary waves on a sloping bottom

Shoaling of solitary waves with different waveheights for initial undisturbed depth $h_0 = 1m$ to smaller new depth up to $h = 0.1m$ are considered. The maximum waveheights were computed at different locations over the slope $S = 1:35$. Figure 3 shows results for solitary wave of height $0.6m$. It shows that waves crests become steeper while shoaling on the slope. We generally see the reflection of a small amplitude wave when a solitary wave goes through a slope. After carefully measuring waveheights over the different slopes the relative maximum local waveheight H/H_0 versus the relative local depth h_0/h are plotted in Figure 4, where h, h_0, H and H_0 represent the

local water depth, the constant reference water depth, local solitary waveheight and initial solitary waveheight, respectively. For later reference, we define the shoaling rate to be the exponent α if the relation $\frac{H}{H_0} = \left(\frac{h_0}{h}\right)^{\alpha}$ holds.

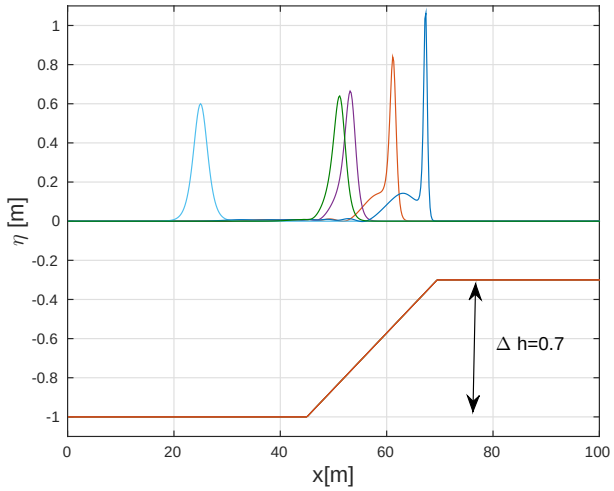

Figure 3: Solitary wave of initial amplitude $0.6m$ transformation on the slope $S = 1 : 35$. Note that the bottom topography is smoothed near the corners.

The effect of a varying bottom on water waves of this class is of obvious engineering importance and numerical solutions have been obtained by Peregrine [35] and Madsen and Mei [25] using a finite difference scheme to compute the deformation of a solitary wave climbing a beach. Experimental results for wave shoaling and breaking of solitary waves were obtained by Ippen and Kulin [17], Kishi and Saeki [22], Camfield and Street [6] and Synolakis [38]. Note also that Pelinovsky and Talipova [33, 34] studied the shoaling curves which were obtained by the waveheight–wave energy relation for numerical solutions of the full water wave problem found by Longuet-Higgins [23], Longuet-Higgins and Fenton [24]. In case of a periodic sequence of solitary waves, Ostrovsky and Pelinovsky [32] found that the shoaling relation reduces to a "nonlinear" Green's law. Recently the experimental results of Grilli et al. [15] and numerical studies based on potential flow theory for the Euler equations, which was presented by Grilli et al. [16] have concentrated on shoaling studies. Noteworthy is the fact that the studies of Grilli et al. [15, 16] gives a nice picture of different shoaling regimes and predict a variety of scaling relations for the local wave amplitude ahead and beyond the breaking point.

For comparison, we have considered the Grilli et al. [16] numerical results. Figure 4 shows plots of data taken from [16]. The shoaling curve for initial amplitudes 0.6 , 0.4 and 0.2 are plotted. The Green's law, which predicts shoaling rates (amplitude increase) $\propto h^{-1/4}$ is plotted with 'G' mark and the Boussinesq's law which gives shoaling rates $\propto h^{-1}$ is plotted with 'B' mark. Figure 4 shows the shoaling curves of the current work are in good agreement with the numerical results of Grilli et al. [16]. It can be seen that the shoaling rate increases initially more slowly than predicted by Green's law, but then increases as the water depth keeps decreasing. Although there is no breaking point in our numerical calculation, it is noticed that the breaking points appeared in the results obtained by Grilli et al. [16]. For instance, (21) is used to check the breaking criterion as discussed above.

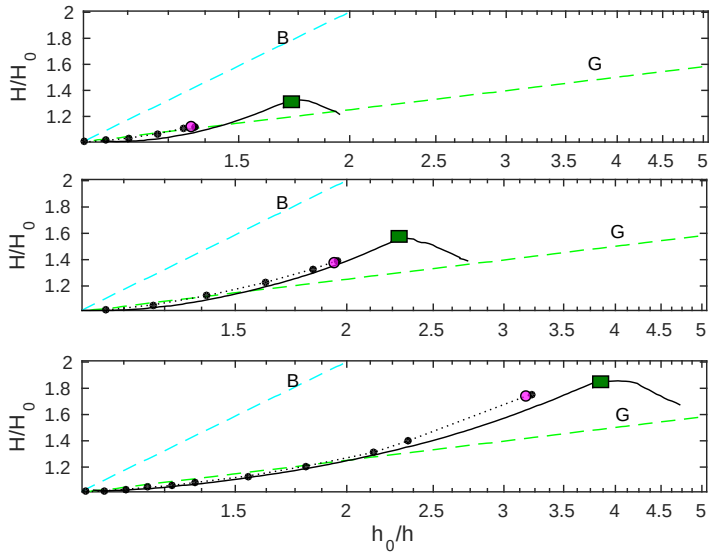

Figure 4: Computations for the shoaling curves with initial amplitudes = 0.6 (upper panel); 0.4 (middle panel); 0.2 (lower panel) on a slope 1:35. Here G denotes Green's law, B denotes Boussinesq's law, the dotted curves are our numerical results and the solid curve are numerical results from Grilli et al. [16] . Rectangular and circular symbols denote the breaking points of Grilli et al. [16] and present work respectively.

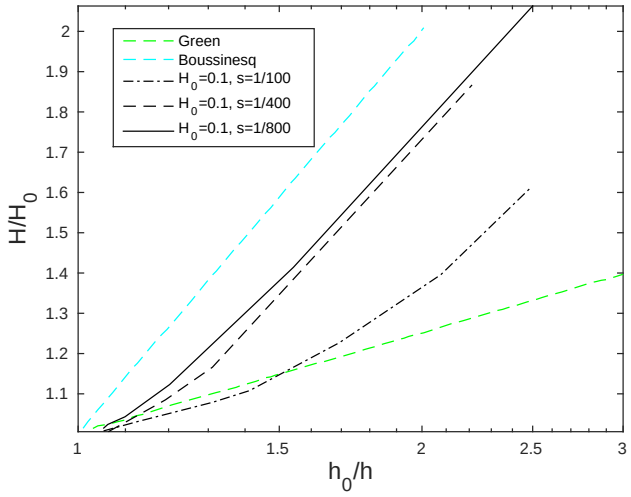

Figure 5: Computations for the shoaling curves with initial amplitude 0.1 on different slopes $1:100$, $1:400$ and $1:800$. Here the solid curve represents the shoaling curve for the slope $1:800$, the dashed curve represents the shoaling curve for the slope $1:400$ and the dotted curve represents the shoaling curve for the slope $1:100$.

Figure 5 shows plots of shoaling rates for wave of initial waveheight 0.1 with different slopes $1:100$, $1:400$ and $1:800$. It is apparent that for slope $1:100$, the shoaling rate is lower than Green's law for small h_0/h and higher for large h_0/h. But for the smaller slopes $1:400$ and $1:800$, the shoaling rate is closer to the line h^{-1} for large h_0/h. Apparently, the computed curves

get close to Boussinesq's law for smaller slopes.

Now the breaking criterion (21) is applied to the solitary wave solutions. In order to find wave breaking in these solitary wave solutions, the x-location of the maximum waveheight at each time step is found. The propagation speed U is then estimated using these x-locations at each time step. Finally if the computed horizontal velocity u exceeds the mean propagation speed U, we can conclude that, around this time step, the wave is starting to break. The water depth at breaking measured under the wave crest is denoted as h_b and the corresponding solitary waveheight at breaking is denoted as H_b. In Table 8 the relative breaking waveheight H_b/h_b at the corresponding breaking points is compared with those of Grilli et al. [16] and Chou et al. [11]. For a large wave amplitude the waveheight will exceed the breaking criterion very soon after it propagates on the slope and so wave breaking occurs almost instantly without too much change in height. The ratio of relative breaking waveheight is larger for small amplitude waves than for large amplitude waves. Wave breaking occurs sooner for larger initial waves.

McCowan [28] theoretically defined the breaker depth index as $H_b/h_b = 0.78$ for a solitary wave traveling over a horizontal bottom using the assumption that instability is reached when the particle velocity at the crest equals the wave celerity and that the crest angle is then 120°. To estimate the initial breaking waveheight on a mild-slope beach, this value ($H_b/h_b = 0.78$) is most commonly used in engineering practice as a first estimate. Ippen and Kulin [17] showed that the upper limit of the breaking criterion should be 0.78 for solitary wave over very mild slope. In this article the slope 1:35 is used and it can be seen from Table 8 that the relative breaking waveheights H_b/h_b are smaller for higher amplitude waves. It is noticed that the relative breaking waveheights H_b/h_b at breaking points are well above the McCowan limit 0.78. Since the relative breaking waveheights H_b/h_b at breaking points are smaller than those obtained by Grilli et al. [16] and Chou et al. [11], we might consider higher order Boussinesq model for further study.

H_0	H_b/h_b			H_b/h_0		
	Chou	Grilli	Present	Chou	Grilli	Present
0.2	1.330	1.402	1.132	0.402	0.364	0.3513
0.25	1.314	1.385	1.056	0.465	0.422	0.3984
0.3	1.283	1.380	1.033	0.514	0.476	0.4475
0.4	1.26	1.378	0.977	0.614	0.592	0.5320

Table 8: Comparison of the relative breaking waveheight for waves with initial amplitudes 0.2, 0.25, 0.3, 0.4 on slope 1:35.

3.4 Comparison of mild slope model systems and results

For comparison, the work of Chen [8] is considered. Chen presented equations for bi-directional waves over an uneven bottom, which may be written in non-dimensional, unscaled variables and disregard terms of order $\mathcal{O}(\alpha\beta, \beta^2)$ as

$$u_t + g\eta_x + uu_x - \frac{1}{2}\left(1-\theta^2\right) {h_0}^2 u_{xxt} = 0, \tag{28a}$$

$$\eta_t + (\eta u + hu)_x - \frac{1}{2}\left(\theta^2 - \frac{1}{3}\right) {h_0}^2 \eta_{xxt} = 0. \tag{28b}$$

The Chen and Mitsotakis models [8, 30] represent the same type of coupled BBM-type system, derived in the context of the Boussinesq scaling. One can derive a number of special cases of the general Boussinesq system. Since we are interested in coupled BBM-type system, the model of Chen is chosen for comparisons. The above system (28) is solved using the same numerical

technique above. The main difference between the two systems (13) and (28) is approximation of bottom motion. In (13), the bottom motion is nondimensionalized by $\tilde{h} = \frac{h}{h_0}$, and in (28), it is nondimensionalized by $\tilde{h} = \frac{h-h_0}{a_0}$ which is similar to the approximation of wave amplitude η. Figure 6 shows computations for the shoaling curves with initial amplitude $0.4m$. It is noticed that the shoaling curve corresponding to the system (28) lies below the Green's law because of the lower order approximation.

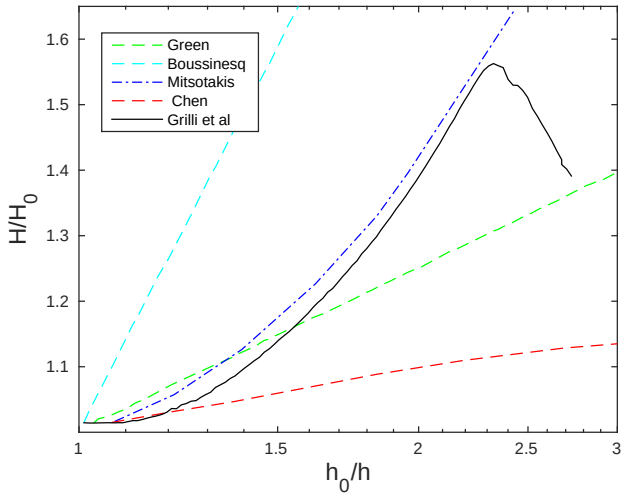

Figure 6: Computations for the shoaling curves with initial amplitude 0.4 on a slope 1:35. Here the dashed - dotted curve represents numerical results for the system (13) derived by Mitsotakis [30], the solid curve are numerical results from Grilli et al. [16] and the dashed curve represents numerical results for the system (28). Indeed the system (28) works for small-amplitude bottom variations as expected, since the bottom function $h(x)$ is assumed to be of order $\mathcal{O}(\alpha)$.

In the paper [8], the bottom function $h(x)$ is assumed to be $\mathcal{O}(\alpha)$ and in the paper [30], the bottom function $h(x)$ is assumed to be $\mathcal{O}(1)$. The results are in line with the assumptions used in their respective derivations.

4 Conclusion

In this article, a coupled BBM system of equations has been studied in the situation of water waves propagating over decreasing fluid depth. A conservation equation for mass and a wave breaking criteria, both valid in the Boussinesq approximation have been found. A Fourier collocation method coupled with a 4-stage Runge-Kutta time integration scheme has been employed in this work to approximate the solution of the BBM system. It has been shown that the approximate mass conservation relation is reasonably accurate. Moreover, the results from evaluation of the approximate mass conservation law show that the ratio of mass reflection to mass influx approaches zero as Δh becomes small.

In our previous paper [19] we showed that for waves of very small amplitude, the shoaling relation approaches Boussinesq's law for Boussinesq-type systems which are valid for waves with the Stokes number $S = \alpha/\beta$ of order 1, and in this case we measured the transition of the wave only at the initial and final stage assuming the wave undergoes an adiabatic adjustment. It is confirmed from Table 7 that the L^2-ratio between reflection and initial solitary wave approaches zero as the slope becomes more and more gentle which lends additional credibility to shoaling

results based on adiabatic approximation. In addition the results displayed in Figure 5 indicate that shoaling rates for small amplitude waves are closer to Boussinesq's law for very gentle slopes.

Considering shoaling of finite amplitude waves, we have compared shoaling curves obtained with the current method to numerical results of Grilli et al. [16] for the Euler equations based on potential flow theory, and the corresponding shoaling curve of the current work is in good agreement with the numerical results of Grilli et al. [16] and it has been found that the variation in waveheight of a shoaling solitary wave initially increases at a lower rate than that predicted by Green's law, but then increases similar to Boussinesq's law. Indeed, the shoaling curves achieved in this paper matches the shoaling curves of Grilli et al. [16] better than the similar approximation established by Khorsand and Kalisch [21].

The comparison of shoaling curves of two model systems (13) ([30]) and (28) ([8]) with the numerical results of Grilli et al. [16] showed that each of these models works well in their respective regimes of applicability.

Acknowledgement

I would like to thank my supervisor, Professor Henrik Kalisch for his helpful guidance, comments and detailed correction on this work. This research was supported by Research council of Norway.

References

[1] A. Ali and H. Kalisch, Mechanical balance laws for Boussinesq models of surface water waves, J. Nonlinear Sci., 2012, 22, 371–398.

[2] A. Ali and H. Kalisch, On the formation of mass, momentum and energy conservation in the KdV equation, Acta Appl. Math., 2014, 133, 113–131.

[3] T.B. Benjamin, J.B. Bona and J.J. Mahony, Model equations for long waves in nonlinear dispersive systems, Philos. Trans. Roy. Soc. London, 1972, A 272, 47–78.

[4] M. Bjørkavåg and H. Kalisch, Wave breaking in Boussinesq models for undular bores, Physics Letters A, 2011, 375, 1570–1578.

[5] J.L. Bona, M. Chen and J.C. Saut, Boussinesq equations and other systems for small-amplitude long waves in nonlinear dispersive media. I: Derivation and linear theory, J. Nonlinear sci., 2002, 12, 283–318.

[6] F. E. Camfield and R. L. Street, Shoaling of solitary waves on small slopes, J. Water. Harb. Coastel Engrg., 1969, 95, 1–22.

[7] M. Chen, Exact solutions of various Boussinesq systems, Appl. Math. Lett., 1998, 11, 45–49.

[8] M. Chen, Equations for bi-directional waves over an uneven bottom, Mat. Comp. Simul., 2003, 62, 3–9.

[9] C.R. Chou and K. Quyang, The deformation of solitary waves on steep slopes, J. Chinese Ins. Engineers. 1999a, 22, 6, 805–812.

[10] C.R. Chou and K. Quyang, Breaking of solitary waves on uniform slopes, China Ocean Engrng. 1999b, 13, 4, 429–442.

[11] C.R. Chou, R.S. Shih and J.Z. Yim, Numerical study on breaking criteria for solitary waves, China Ocean Engrng., 2003, 17, 4, 589–604.

[12] J.H. Duncan, Ann. Rev. Fluid Mech., 2001, 33, 519–547.

[13] D. Gottlieb and S.A. Orszag, Numerical Analysis of Spectral Methods: Theory and applications, SIAM, Philadelphia, 1986.

[14] A.E. Green and P.M. Naghdi, A derivation of equations for wave propagation in water of variable depth, J. Fluid Mech., 1976, 78, 237–246.

[15] S. T. Grilli, R. Subramanya, I.A. Svendsen and J. Veeramony Shoaling of solitary waves on plane beaches, J. Waterway, Port, Coastal and Ocean Engrng., 1994, 120 , 609–628.

[16] S. T. Grilli, I.A. Svendsen and R. Subramanya, Breaking criterion and characteristics for solitary waves on slopes, J. Waterway, Port, Coastal and Ocean Engrng., 1997, 123 , 102–112.

[17] A. T. Ippen and G. Kulin, The shoaling and breaking of the solitary wave, Proc. 5th Conf. on Coastal Engineering, 1954, 27–47.

[18] R.S. Johnson, On the development of a solitary wave moving over uneven bottom, Proc. Cambridge Philos. Soc., 1973, 73, 183–203.

[19] H. Kalisch and A. Senthilkumar, Derivation of Boussinesq's shoaling law using a coupled BBM system, Nonlin. Processes Geophys., 2013, 20, 213–219.

[20] A.B. Kennedy, Q. Chen, J. T. Kirby, and R.A. Dalrymple, Boussinesq modeling of wave transformation, breaking, and runup. I: 1D, J. Waterway, Port, Coastal and Ocean Engrng., 2000, 126, 39–47.

[21] Z. Khorsand and H. Kalisch, On the shoaling of solitary waves in the KdV equation, Proceedings of 34th Conference on Coastal Engineering, Seoul, Korea, 2014, 34.

[22] T. Kishi and H. Saeki, The shoaling, breaking and runup of the solitary wave on impermeable rough slopes. Proc. 10th Con. Coastal Engng., 1966, 1, 322.

[23] M.S. Longuet-Higgins, On the mass, momentum, energy and circulation of a solitary wave, I, P. Roy. Soc. Lond. A Mat., 1974, 337, 1–13.

[24] M.S. Longuet-Higgins and J.D. Fenton, On the mass, momentum,energy and circulation of a solitary wave. II, P. Roy. Soc. Lond.A Mat., 1974, 340, 471–493.

[25] O.S. Madsen and C.C. Mei, The Transformation of a solitary wave over an uneven bottom, J.Fluid Mech., 1969, 39, 781–791.

[26] P.A. Madsen, R. Murray and O.R. Sørensen, A new form of the Boussinesq equations with improved linear dispersion characteristics, Coastal Engineering, 1991, 15, 4, 371–388.

[27] P.A. Madsen and H.A. Schäffer, Higher-order Boussinesq-type equations for surface gravity waves: derivation and analysis, Phil. Trans. R. Soc. Lond. A, 1998, 356, 3123–3184.

[28] J. McCowan, On the highest wave of permanent type, Philos. Mag., 1894, 38, 351–357.

[29] J.W. Miles, On the Korteweg–de Vries equation for a gradually varying channel, J.Fluid Mech., 1979, 91, 181–190.

[30] D.E. Mitsotakis, Boussinesq systems in two space dimensions over a variable bottom for the generation and propagation of tsunami waves, Mat. Comp. Simul., 2009, 80, 860–873.

[31] O. Nwogu, Alternative form of Boussinesq equations for nearshore wave propagation, J. Waterway, Port, Coastal and Ocean Engrng., 1993, 119, 618–638.

[32] L.A. Ostrovsky and E.N. Pelinovsky, Wave transformation on the surface of a fluid of variable depth, Atmospheric and Oceanic Physics, 1970, 6, 552–555.

[33] E.N. Pelinovsky and T.G. Talipova, Height variations of large amplitude solitary waves in the near-shore zone, Oceanology, 1977, 17, 1–3.

[34] E.N. Pelinovsky and T.G. Talipova, Change of height of the solitary wave of large amplitude in the beach zone, Mar. Geodesy, 1979, 2, 313–321.

[35] D.H. Peregrine, Long waves on a beach, J.Fluid Mech., 1967, 27, 815–827.

[36] A. Senthilkumar, BBM equation with non-constant coefficients, Turk J Math., 2013, 37, 652–664.

[37] I.A. Svendsen, Introduction to nearshore hydrodynamics, World Scientific, Singapore, 2006

[38] C.E. Synolakis, The runup of solitary waves, J. Fluid Mech., 1987, 185, 523–545.

[39] M.H. Teng and T.Y. Wu, Evolution of long water waves in variable channels, J. Fluid Mech., 1994, 266, 303–317.

[40] L.N. Trefethen, Spectral methods in Matlab, SIAM, Philadelphia, 2000.

[41] G. Wei, J. T. Kirby, S. T. Grilli and R. Subramanya, A fully nonlinear Boussinesq model for surface waves. I. Highly nonlinear, unsteady waves, J. Fluid Mech., 2012, 294, 71–92.

[42] G. Whitham, Linear and nonlinear waves, Wiley-Interscience, New York, 1974.